Biophysical Journal Volume 75 December 1998 2743–2756

System for Dynamic Measurements of Membrane Capacitance in Intact Epithelial Monolayers

C. A. Bertrand,*# D. M. Durand,# G. M. Saidel,# C. Laboisse,§ and U. Hopfer*
Departments of *Physiology and Biophysics and #Biomedical Engineering, Case Western Reserve University, Cleveland, Ohio 44106 USA, and §INSERM 94-04, Universite de Nantes, F-44035 Nantes, France

ABSTRACT Dynamic measurements of exocytosis have been difficult to perform in intact epithelial monolayers. We have designed a system that estimates with ±1% accuracy (99% confidence) the total membrane capacitance of monolayers represented by a lumped model. This impedance measurement and analysis system operates through a conventional transepithelial electrophysiology clamp, performing all signal measurements as frequently as every 5 s. Total membrane capacitance (the series combination of apical and basolateral membranes) is the inverse of one of three unique coefficients that describe the monolayer impedance. These coefficients are estimated using a weighted, nonlinear, least-squares algorithm. Using the estimated coefficients, solution ranges for individual membrane parameters are calculated, frequently providing results within ±20% of true values without additional electrophysiological measurements. We determined the measurement system specifications and statistical significance of estimated parameters using 1) analytical testing with circuit simulation software and equation-generated data; 2) a system noise analysis combined with Monte Carlo simulations; and 3) analog model circuits for calibration of the electronic system and to check equation-generated results. Finally, the time course of capacitance changes associated with purinergically stimulated mucin exocytosis are quantified in monolayers of the colonic goblet cell-like cell line HT29-Cl.16E.

INTRODUCTION

Substantial progress has been made in identifying key elements of the exocytotic signaling pathway in neurosecretory cells. Recent efforts have begun to identify many similar proteins and mechanisms in epithelial cells (Peng et al., 1997; Low et al., 1996; Gaisano et al., 1996; Riento et al., 1996). However, the control of these pathways and their coupling to electrolyte secretion in epithelial cells is still poorly understood. One of the reasons for this slow progress with epithelia is that technologies developed to investigate the dynamic behavior of exocytosis in neurosecretory cells, such as whole-cell patch-clamp capacitance measurements, are difficult to apply to intact epithelial monolayers. 1) For example, the role of intact monolayer properties in exocytosis, such as cell-to-cell communication, gap junctions, and membrane polarity cannot be tested with these methods. 2) Differences in the rates of exocytosis and endocytosis between isolated cells and intact monolayers have been shown by recent work in this laboratory on the epithelial cell line HT29 (Guo et al., 1997; Merlin et al., 1994). 3) Furthermore, a significant error can be projected into the capacitance measurement when exocytosis occurs simultaneously with large or rapid changes in membrane conductance (Debus et al., 1995; Barnett and Misler, 1997).

The Cl.16E subclone of the HT29 cell line forms a confluent monolayer and differentiates to a Cl^--secreting cell possessing multiple Cl^- conductances under control by different cellular signaling systems (Guo et al., 1995; Merlin et al., 1994, 1996). In addition, this goblet-cell-like subclone contains large numbers of granules in the apical cytoplasm that undergo compound exocytosis and release mucin upon stimulation with purinergic, vasoactive intestinal peptide, or cholinergic agonists (Laburthe et al., 1989; Merlin et al., 1994; Roumagnac and Laboisse, 1987). Whole-cell patch-clamp measurements of capacitance in subconfluent, isolated Cl.16E cells after purinergic stimulation indicate massive granule fusion followed by complete endocytosis in less than 1 min (Guo et al., 1997). In contrast, experiments with labeled granule contents (Merlin et al., 1994) and preliminary work using impedance analysis (Bertrand et al., 1996) indicate that the peak of exocytosis occurs between 1 and 5 min, and endocytosis lasts 10–15 min in intact monolayers.

Impedance analysis techniques have been used to measure the static properties of a variety of intact monolayers of epithelial cells (Clausen et al., 1979, 1981; Kottra and Frömter, 1984a,b). Major problems exist with the technique, however, and have made it particularly difficult to apply to measurement of dynamic monolayer responses. The number of membrane parameters of even the simplest intact monolayer model exceeds the information contained in the measured impedance. Additional information is typically acquired with microelectrode impalements (Kottra and Frömter, 1984a,b) or membrane permeabilization (Wills et al., 1979). These additional measurements can be difficult to apply, may not predict the variation in a membrane parameter through the dynamics of an experiment, and are often

Received for publication 18 February 1998 and in final form 12 August 1998.

Address reprint requests to Dr. Ulrich Hopfer, Department of Physiology and Biophysics, S.O.M. E566, Case Western Reserve University, 10900 Euclid Avenue, Cleveland, OH 44106-4970. Tel.: 216-368-2878; Fax: 216-368-3952; E-mail: uxh@po.cwru.edu.

0006-3495/98/12/2743/14 $2.00

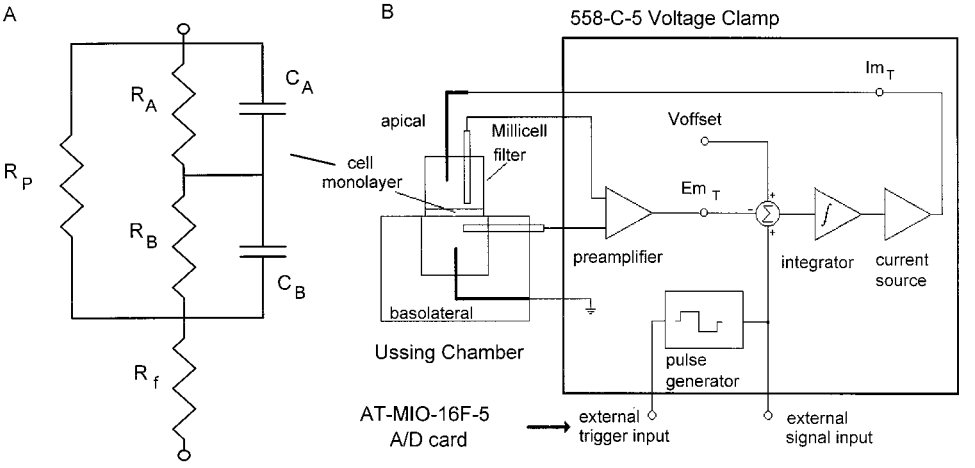

FIGURE 1 (*A*) Lumped-model of the intact epithelial monolayer. A refers to apical, B to basolateral, and P to paracellular pathways; R_f is the extracellular fluid resistance. (*B*) Schematic of the impedance measurement system, including the transepithelial voltage clamp components. Measurement points are Em_T and Im_T.

the limiting factor in the accuracy of membrane parameter estimates. To characterize complex epithelia, distributed models have been developed (Clausen et al., 1979) that, although providing more detailed descriptions of cell structure, increase the number of undefined parameters. Solving these types of models requires further simplifying assumptions as well as specialized stimulus signals. These requirements are difficult to satisfy in a dynamic process where single-point measurement times must be short enough such that the parameters can be considered time invariant, and several parameters are expected to change over the full time course of an experiment.

To overcome the limitations of previous implementations, we have developed a new, optimized method for dynamic impedance measurements and analysis. This method is applied to determine rates of stimulated exocytosis and endocytosis in intact HT29-Cl.16E monolayers, a homogeneous epithelium that, as with previously tested colonic epithelia (Clausen and Wills, 1981; Wills and Clausen, 1987), can be adequately modeled using a simple, lumped model. Two specific areas are addressed: the electronic implementation of the system (measurement) and the estimation technique (analysis). The impedance measurement is performed with a transient pulse as a stimulus and coupled with a standard transepithelial electrophysiology clamp. The short-circuit technique (Schultz, 1980) is used to simultaneously monitor net charge flux. The system performs signal measurements for impedance determination in less than 1 s, followed by signal measurements for transepithelial total resistance determination; complete signal measurements can be performed as frequently as every 5 s.

The parameter estimation is performed off-line in two steps. 1) The coefficients of the impedance equation (impedance coefficients), which are uniquely defined, are estimated using a nonlinear least squares algorithm (Press et al., 1986). The inverse of one of these impedance coefficients defines total monolayer capacitance, providing a direct measure of exocytosis without the need for any additional measurements. 2) Using the impedance coefficient estimates, feasible membrane resistance and capacitance parameter estimates are calculated, defining the ranges in which the true values lie. In many cases, these ranges define the membrane parameters with better precision than traditional techniques using auxiliary measurements.

SYSTEM THEORY

Model

The HT29-Cl.16E intact monolayer can be described by a lumped model (Fig. 1 *A*) with five parameters: R_A, C_A and R_B, C_B, the resistance and capacitance of the apical and basolateral membranes, respectively, and R_P, the resistance of the paracellular pathway. The model relates these membrane parameters to Im_T and Em_T, the measured values for current through and voltage across the monolayer and external fluid, and to the fluid resistance R_f. These variables can be combined (Appendix A) to define the total impedance Z_T of the monolayer (Z_m) and fluid (R_f):

$$Em_T(s)/Im_T(s) = Z_m(s) + R_f = Z_T(s) \tag{1}$$

The transepithelial total resistance R_T is measured at DC conditions and corresponds to the value of $Z_T(s)$ in Eq. 1 when $s = 0$:

$$R_T = \left(\frac{1}{R_p} + \frac{1}{R_A + R_B}\right)^{-1} + R_f \equiv R_m + R_f \tag{2}$$

Using Eq. 2 to reduce the number of parameters to four and substituting the parameter values as detailed in Appendix A gives:

$$Z_T(s) = \frac{N1s + N0}{s^2 + D1s + N0/R_m} + R_f, \tag{3}$$

where the three impedance coefficients are:

$$N1 = \frac{1}{C_A} + \frac{1}{C_B} \tag{4a}$$

$$N0 = \left(\frac{1}{R_A} + \frac{1}{R_B}\right)\frac{1}{C_A C_B} \quad (4b)$$

$$D1 = N1\left(\frac{1}{R_m} - \frac{1}{R_A + R_B}\right) + \frac{1}{R_A C_A} + \frac{1}{R_B C_B} \quad (4c)$$

From measurements of $Z_T(s)$, R_f, and R_T ($R_m = R_T - R_f$), the impedance coefficients can be uniquely estimated.

Modifications to transepithelial electrophysiology

A transepithelial voltage clamp system is shown in Fig. 1 *B* (see Experimental Methods for system details) with the measurement points Em_T and Im_T indicated. The traditional mode of operation to assess active net transepithelial charge transport is the short-circuit mode, where $Em_T(t) = 0$ and $Im_T(t) = Isc$. The transepithelial total resistance (R_T) is determined by applying a known step in control voltage (ΔE) of sufficient width ($\geq$0.5 s) to approximate DC conditions and measuring the change in current (ΔI). In the short-circuit mode, only the changes reflect monolayer and fluid resistance:

$$R_T = \frac{\Delta E}{\Delta I} = \frac{Em_T(t) - 0}{Im_T(t) - Isc}$$

If the step in control voltage approximates an impulse function $\delta(t)$, the resulting changes in membrane potential and current provide a measure of $Z_T(s)$. An impulse can be approximated by a short pulse with a width that is very small with respect to the characteristic frequencies of the system being analyzed (Gabel and Roberts, 1980). Performing both measurements sequentially provides additional information needed to solve the estimation problem. 1) As described above, the measured value of R_T is used to reduce the unknown membrane parameters to 4; 2) the 0 (DC) frequency component of $Z_T(s)$ can be replaced by R_T, eliminating the need to manipulate the measured signals for bias correction, i.e., the subtraction of *Isc* bias from $Im_T(t)$. This approach is valid when the elapsed time between impulse and DC pulse is sufficiently short.

Eq. 5 defines Z_x, the measured value of the impedance $Z_T(s)$ in terms of the fast Fourier transforms (FFTs) of the measured signals $Em_T(t)$ and $Im_T(t)$ and R_T:

$$Z_x(s) = FFT(Em_T(t))/FFT(Im_T(t)) \quad (5)$$

with $Z_x(s)|_{s=0} = R_T$.

EXPERIMENTAL METHODS

Cell culture

HT29-Cl.16E cells were propagated in Falcon (Becton-Dickinson, Franklin Lakes, NJ) culture flasks (25 cm^2) in a humidified atmosphere of 95% air and 5% CO_2 at 37°C. The cells were fed daily with Dulbecco's modified Eagle's medium (Gibco-BRL, Grand Island, NY) supplemented with 10% heat-inactivated fetal bovine serum (Gibco-BRL) and 4 mM L-glutamine (Gibco-BRL). Cultures were periodically tested for mycoplasma (Chen, 1977). The passage numbers for the reported experiments were between 35 and 50.

Cell monolayers for electrophysiology were grown on Vitrogen-coated (Collagen Corp., Palo Alto, CA), Millicell-CM (Millipore, Bedford, MA; size 12mm) filters. Cl.16E cells were seeded at a density of 1.2×10^6/filter (0.6 cm^2 per filter). Cells became visually confluent after 7 days and were used for electrophysiology studies between days 12 and 20.

Transepithelial electrophysiology

DC measurements

Transepithelial electrophysiology measurements were performed using an Ussing-type chamber modified to accept the Millicell filters (Analytical Bioinstrumentation, Cleveland, OH; see Fig. 1 *B*). The chamber was equipped with a conventional four-electrode system connected to a voltage clamp (model 558-C-5, University of Iowa Bioengineering, Iowa City, IA). All measurements were made in the short-circuit mode (transepithelial potential Em_T clamped to 0 V) unless noted; short-circuit current (*Isc*) and R_T were monitored. To measure R_T, Em_T was pulsed $\pm$2.0 mV for 1 s using an external trigger of the voltage clamp pulse generator. Voltage reference electrode offset (*V*offset) and fluid resistance (R_f) were measured at the start of each experiment using a blank Millicell filter perfused with the desired solution. *V*offset was compensated. Positive currents correspond to anion secretion/cation absorption (lumen negative potential under open circuit conditions). The Ussing chamber and all solutions were maintained in an incubator at 37°C and 5% CO_2. Apical and basolateral chambers were perfused separately.

Impedance measurements

The impedance measurement consisted of simultaneous signal generation and two-channel analog acquisition. All pulse generation, data acquisition, and timing were performed using an AT-MI0-16F-5 A/D card (National Instruments, Austin, TX) installed in a PC (486DX at 60 MHz). Pulse and trigger signals were applied to the external (command) signal input of the 558-C-5 voltage clamp or the external trigger input of the 558-C-5 voltage clamp pulse generator. The determination of the pulse and acquisition characteristics and estimation of capacitance are the subject of the rest of the paper.

Protocols

Exocytosis was stimulated in Cl.16E monolayers using the purinergic agonist ATP (Merlin et al., 1994). The protocol was designed to monitor the time course of exocytosis and

endocytosis. After a 30-min incubation in slightly hypertonic (110% of normal) Ringer's solution (114 mM NaCl, 4 mM KCl, 1 mM $MgCl_2$, 1.25 mM $CaCl_2$, 22.98 mM $NaHCO_3$, 31.7 mM sucrose, and 25 mM D-glucose at pH 7.4), measurements of basal impedance and R_T were performed. After 10 min, a bolus of ATP (18 μl of 10^{-1} M for a final concentration of 3 mM) was added directly to the apical chamber. Measurements of impedance and R_T were continued for 25 min after stimulation. These data were then analyzed to estimate the impedance coefficients.

For preliminary measurements of the resistance ratio of apical to basolateral plasma membrane, either apical or basolateral membrane permeabilization experiments were performed with the ionophore amphotericin B (at a final concentration of 20 μM in 0.1% dimethylsulfoxide) as previously described (Merlin et al., 1994). Unless noted, all chemicals were purchased from Sigma (St. Louis, MO).

RESULTS

Implementing the impedance measurement

Preliminary evaluation of parameters

Knowledge of expected membrane parameter ranges is crucial to the design of the measurement and analysis systems, as they define the critical stimulus frequencies and place limits on the estimation results. To this end, values of minimal and maximal capacitance and resistance of HT29 monolayers were determined based on morphological data, membrane permeabilization experiments, total resistance measurements, and preliminary experimental data. Values normalized to macroscopic monolayer area are given in Table 1. Minimal values for surface areas are derived by considering cells as cylinders with smooth, nonfolded plasma membranes and estimating height-to-diameter ratios of cells from electron micrographs (Merlin et al., 1994). Applying this technique, the minimal apical capacitance is fixed by filter size and the assumption of a specific membrane capacitance of 1 μF/cm^2 (Cole, 1968); the minimal basolateral capacitance is calculated as 5 μF/cm^2. The upper limits were determined from preliminary data (Bertrand et al., 1996).

The minimal and maximal values of total resistance R_T listed in Table 1 were measured in HT29-Cl.16E monolayers ($n = 50$) during purinergic stimulation tests. To estimate relative resistance ratios for apical and basolateral membranes, one of the membranes was permeabilized with amphotericin B (basal conditions). Although this technique does not provide absolute values for any of the resistances, it substantially decreases the resistance of the permeabilized membrane. From the relations in Eq. 2, the relative contribution of either R_A or R_B to the total resistance R_T can be estimated. Permeabilizing the apical membrane dramatically reduced the total resistance of the monolayer to 20% (on average, $n = 10$) of the total. The same treatment to the basolateral membrane produced a much smaller decrease in total resistance to 80% (on average, $n = 20$) of the total. From these results, the ratio of apical to basolateral resistance under basal conditions was estimated to be at least 2. Finally, the sum of apical and basolateral membrane resistances ($R_A + R_B$) as well as the paracellular resistance R_P must both be greater than R_m ($\equiv R_T - R_f$) for their values to be positive.

TABLE 1 Limits on membrane parameters

Parameter	Minimum	Maximum
C_A (μF/cm^2)	1.0	5.0
C_B (μF/cm^2)	5.0	25.0
R_A (Ω cm^2)	300	1800
R_B (Ω cm^2)	30	450
R_P (Ω cm^2)	200	900
R_T (Ω cm^2)	125	640

Values of R_T are from direct measurements.

Frequency response and circuit simulations

To design the appropriate stimulus pulse for impedance measurements, it is necessary to determine the characteristic frequencies of the epithelial monolayer. The frequency range over which $Z_T(s)$ is most sensitive to changes in the impedance coefficients can be determined by calculating the relative sensitivity functions $SF_j = \partial Z_T(s)/\partial(\ln\theta_j)$, $j = 1, 2, 3$ where $\theta = [N1, N0, D1]$. Fig. 2 shows the real and imaginary components of the complex sensitivities corresponding to basal conditions of HT29 monolayers. The impedance is most sensitive to changes in $D1$ and least sensitive to $N0$. All sensitivities peak under 1000 Hz. Testing the sensitivities with coefficient values expected during purinergic stimulation shifts the peak sensitivities to lower frequencies but does not substantially alter the shape or amplitudes of the response (data not shown).

Pulse and acquisition specifications

Several factors must be considered in specifying the acquisition characteristics. First, the stimulus pulse must be short with respect to the characteristic frequencies of the monolayer. From the results above, the epithelial monolayer peak sensitivity is $\leq$1000 Hz; the desired stimulus pulse spectra must contain frequencies at least 10 times this frequency. Second, the minimal frequency should be high enough ($>$10 Hz) to avoid electrode polarization effects (Geddes and Baker, 1967). Third, the range of signals should be predominantly in the linear range of the transepithelial clamp response, measured as 10 Hz to 10 kHz (data not shown). Fourth, the constraints of digital acquisition and transforms must be considered. The transforms in Eq. 5 require that 2^n data points be collected, where n is an integer. In addition, the output stimulus is synchronized with analog acquisition, so that the width of the output pulse must be an integer multiple of the sampling rate. Fifth, the signal amplitude should be small enough to minimally perturb the monolayer while maintaining a useable signal-to-

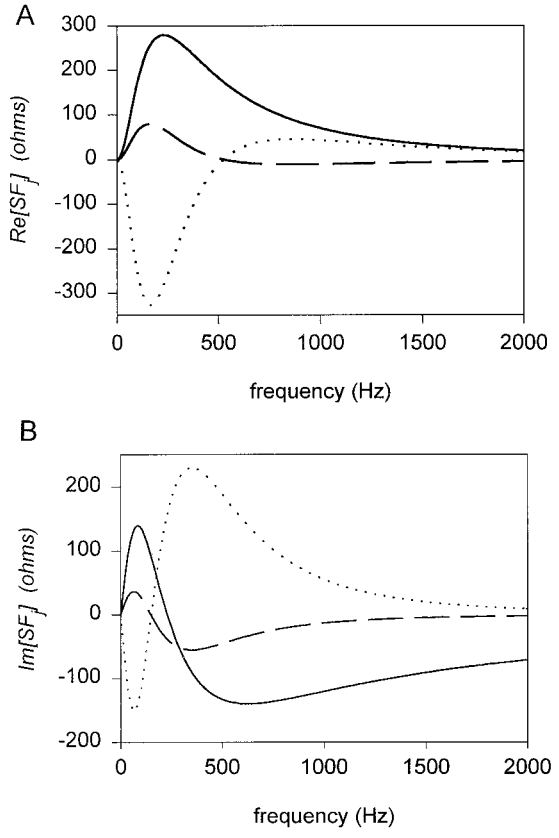

FIGURE 2 Plot of the relative sensitivity functions SF_j as a function of frequency. The SF_j show the sensitivity of the total impedance Z_T to changes in the impedance coefficients of Eq. 3. (*A*) the real components of SF_j; (*B*) the imaginary components of SF_j. The impedance coefficients were chosen to represent HT29-Cl.16E monolayers under basal conditions, with $N1 = 0.954$ (——), $N0 = 7.81 \times 10^{-4}$ (— —), *and* $D1 = 3.41 \times 10^{-3}$ ($\cdots$).

noise ratio. Finally, techniques for noise reduction must be employed. In addition to signal averaging, the sampled frequencies can be chosen to isolate the 60-Hz line frequency and its harmonics, so that large deviations in these signals (i.e., noise; see below) are clearly identified and correctly weighted in the estimation process.

With these factors considered, the specifications of the acquisition process were defined as follows. The signals $Em_T(t)$ and $Im_T(t)$ were acquired at a rate of 24.6 k samples/s, 2250 samples total; the first 202 samples were discarded to give 2048 samples, providing frequency samples from 12 Hz to approximately 12 kHz in 12-Hz increments. The stimulus pulse was one sample (40.7 μs) wide and filtered (four-pole, Butterworth low-pass with $f_c = 11$ kHz) before application to the external signal input of the clamp; the pulse was generated on the 204th sample. The stimulus pulse amplitude across the monolayer was optimally 7.5 mV, well within the linear IV response of HT29-Cl.16E monolayers (tested to ± 100 mV; data not shown). Sampling with stimulus pulse was repeated eight times consecutively without pause, and the eight data sets were averaged for noise reduction to give one stored data set with a total measurement time of approximately 800 ms.

To test these specifications, $Em_T(t)$ and $Im_T(t)$ were acquired using an analog model circuit with component values chosen to simulate HT29 monolayers. The impedance spectra of $Z_x(s)$ was determined from these measured signals (Eq. 5), and compared with $Z_T(s)$ calculated from the known components (Eq. 3). Using component values to simulate the full range ($n = 10$) of impedances expected (Table 1), the system was found to exhibit a small, constant, frequency-dependent error between Z_x and Z_T, which ranged from 2% at low frequencies to a maximal 5% at the highest frequencies. Circuit simulation tests verified that the error was the result of differences in the frequency response of the amplifiers that process the current and voltage signals, as well as instrumentation biases in the A/D process. From these results, a correction function was generated, which is applied to all collected data.

Noise analysis

The quality of the coefficient estimates depends on several properties of the measurement system. As previously explained, the acquisition specifications are designed to probe the epithelial monolayer at its characteristic frequencies within the linear response of the clamp and out of the range of electrode polarization effects. Other factors to be considered are noise present in the measured signal and how it can be minimized through system design techniques and accounted for with weighted estimation. The analog model circuit was used to assess noise components present in the measurement system. First, using the same components, 10 random measurements were performed, the impedance $Z_x(s)$ was determined, and all results were averaged. This averaged impedance was then compared with the individual measurements to determine the standard deviations due to noise (σ_ϵ) at each frequency. The real and imaginary components of the noise standard deviations for a model circuit simulating basal conditions are shown in Fig. 3 *A*.

The noise levels in Fig. 3 *A* represent the expected values after noise reduction techniques (detailed above) were employed. To determine whether the noise pattern evident with the model circuit was comparable to Cl.16E monolayers, the same measurements were performed on monolayers after a stable baseline had been achieved ($n = 20$, at least 10 measurements each). A typical noise plot for Cl.16E monolayers is shown in Fig. 3 *B*. The noise pattern measured in monolayers is similar to that of the analog model circuit, except for larger peaks at the power line frequency and its harmonics. This measurement is performed at the start of each experiment to determine the standard deviations (σ_ϵ) of the measured variables.

The estimation problem

As described earlier, $Z_T(s)$ is fully determined by three unique impedance coefficients, which, in turn, are related to four unknown membrane parameters (Eq. 4, a–c). The first

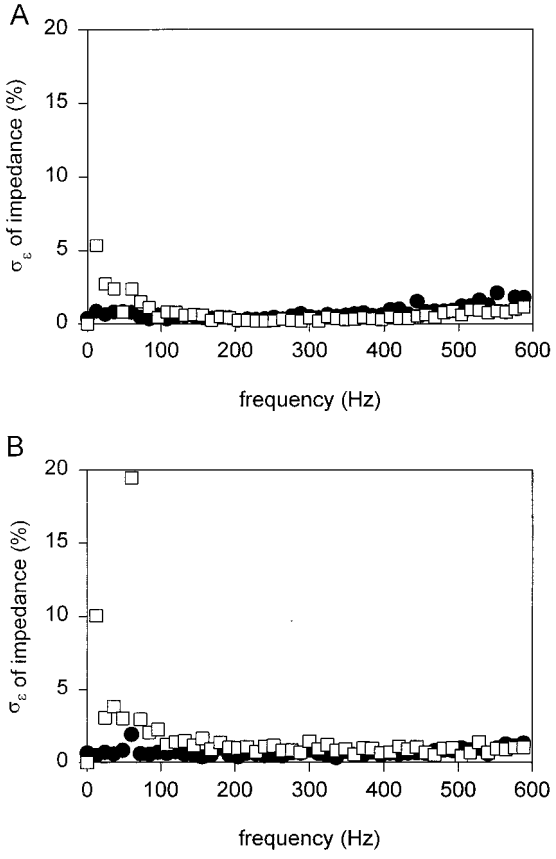

FIGURE 3 The noise spectrum measured in an analog model circuit (*A*) and in HT29-Cl.16E monolayers (*B*). The noise spectra are defined in terms of the percent standard deviations in impedance at each frequency sample. Real components (●) and imaginary components (□) are shown.

step is the estimation of the impedance coefficients. These coefficient estimates provide an immediate result: total monolayer capacitance (Eq. 4a). Next, feasible membrane resistance and capacitance parameter values that fit Eq. 4, a–c, can be calculated using the estimated coefficients, defining the ranges in which the true values lie. As will be shown, the estimated ranges of the membrane parameters by themselves provide useful information on the behavior of the monolayer and can be frequently used to make an educated guess at one of the parameter values. With a guess or measurement of one parameter, the remaining three can be solved using Eq. 4, a–c.

Impedance coefficient estimation

The estimation of the impedance coefficients $N1$, $N0$, and $D1$ can be posed as a nonlinear, weighted, least squares (NWLS) minimization. The best estimate of the coefficient vector $\theta = [N1, N0, D1]^T$ is found by minimizing:

$$\chi^2(\theta) = \sum_{i=1}^{N} (Y_i(\theta))^2 = \sum_{i=1}^{N} (Re(Y_i(\theta)))^2 + \sum_{i=1}^{N} (Im(Y_i(\theta)))^2,$$

where

$$Y_i(\theta) = \frac{Z_{Xi} - Z_{Ti}(\theta)}{\sigma_{\epsilon i}}$$

The weighting factors $\sigma_{\epsilon i}$ = the noise standard deviations of the impedance at the N frequencies. The Levenberg-Marquardt NWLS method (Press et al., 1986) was used to estimate the coefficients.

Tests of the NWLS estimation program were initially performed with equation-generated (Eq. 3) data, both ideal and with added noise. Ideal data resulted in absolute convergence using a wide range of initial guesses. The noise added to data had similar amplitudes and standard deviations as that measured with monolayers (e.g., Fig. 3 *B*) and was generated as described in detail in Appendix B. A typical fit of the impedance spectra generated from noisy data is shown in Fig. 4, along with a plot of the weighted

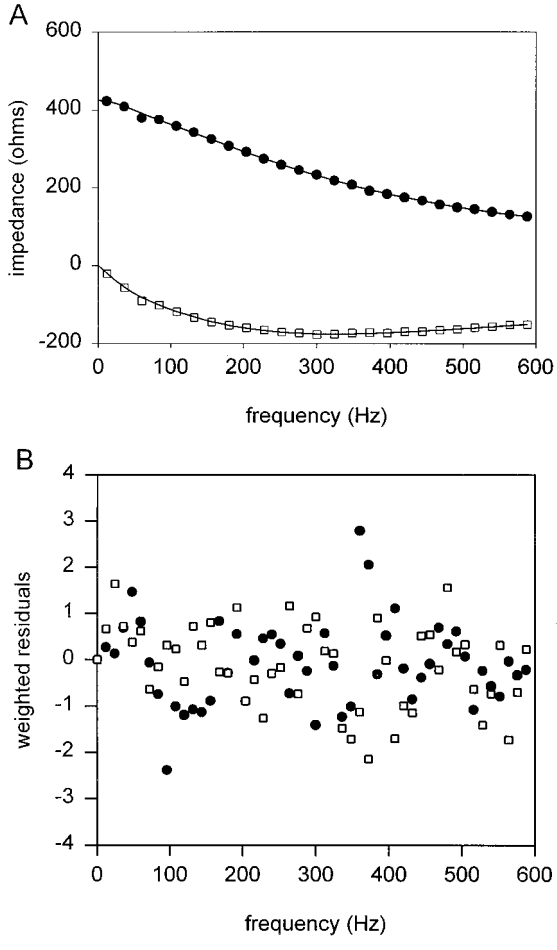

FIGURE 4 Effect of noise on the estimates of the impedance coefficients and resulting impedance fit. (*A*) Real (●) and imaginary (□) components of noisy impedance generated from known coefficients by Eq. 3 plus added noise with characteristics similar to measured noise as detailed in Appendix B; the lines indicate the fitted result extracted from the noisy data by NWLS. (*B*) The real (●) and imaginary (□) components of the weighted residual errors between the generated noisy and the fitted impedances. The weights are assigned 1.5 Ω cm^2, the value of standard deviation used in the noise generation program (Appendix B).

residuals. To quantitatively assess the goodness-of-fit of the estimated parameters and model, several tests were applied. 1) The minimized χ^2 of the fit, with appropriately estimated weights, was calculated. This value should be approximately ν, the degrees of freedom (number of residuals − number of parameters; Press et al., 1986) for an appropriate fit. 2) A runs test was performed on the residuals to quantify any trends that might indicate serial correlation (systematic behavior, Straume and Johnson, 1992a). 3) Finally, a χ^2 goodness-of-fit test was used to compare the residual distributions with a normal distribution (mean = 0 and $\sigma = 1$; Straume and Johnson, 1992a). For all three tests, the estimated parameters generated residuals that fell within a 95% confidence interval, suggesting that the residuals of the fit are normally distributed and free of any systematic errors.

Monte Carlo simulations

The significance of the parameter estimates themselves cannot be predicted from the standard deviations of the fit because the correlation coefficients of $N0$ and $D1$ approach unity (Johnson, 1994). In this case, Monte Carlo simulations are required to determine the confidence intervals of the estimated parameters. To this end, impedance data were generated using coefficient values determined from experiments with HT29-Cl.16E monolayers (presented in greater detail below). Noise was added to the impedance data, and then new values for the coefficients were estimated from the noisy data by NWLS (Straume and Johnson, 1992b). The characteristics and method of addition of noise are described in detail in Appendix B. These simulations were performed with coefficient values from HT29-Cl.16E monolayers in three different states: basal (case 1), 1 min after ATP addition (case 2), and 25 min after ATP addition (case 3). For each case, 250 runs were performed with random noise.

The results are summarized in Table 2. The $N1$ coefficient, which represents the inverse of total monolayer capacitance, has excellent precision. From the histogram of the 30-min post-ATP results in Fig. 5*A*, a normal distribution can be assumed. For a 99% confidence interval, the value of $N1$ will be within ±1% for all three experimental cases indicated in Table 2. Plotting the values of $N1$ as a function of $N0$ and $D1$ indicated minimal correlation (not shown). In addition, correlation to the added mean noise and R_m was minimal.

The results for coefficient $N0$ indicate poor ($\sigma \approx 50\%$) precision for the basal case and acceptable ($\sigma \approx 10\%$) precision for the other cases. Coefficient $D1$, although much improved in tolerance over $N0$, follows the same pattern of error. To assess the degree of correlation and factors affecting the variance in results, the values of $N0$ were plotted as a function of the mean noise, R_m, and $D1$ values. The results, indicated in Fig. 6, show minimal correlation to errors in the mean noise. There is a measure of linear correlation with changes in R_m and a strong degree of linear correlation with $D1$. The correlation of $D1$ with R_m is also shown in Fig. 6 and matches the pattern of $N0$. From Eq. 4, b and c, only $D1$ depends on the value of R_m and is the probable source of the error evident in $N0$. For the post-ATP cases, a 90% confidence interval for $D1$ results in a maximal ±10% variation.

Several of the runs failed to reach convergence in the allowed number of iterations (i.e., case 1, 24 runs, or 9.6%, failed). Failure to converge typically occurred when the mean and standard deviation of the added noise were greater than ±0.5 and 2 Ω cm^2, respectively. Such values are expected to occur occasionally with random number generation (Appendix B). These results suggest failure to converge will also occur with monolayer data having similar bias errors, whether from systematic errors or noise.

Membrane parameter ranges

Once the impedance coefficients are estimated, the membrane parameter ranges can be determined from Eq. 4, a–c. Rearranging Eq. 4a to give Eq. 6, it is clear that the estimated value of $N1$ sets a minimal value for C_A (when $C_B \rightarrow \infty$).

$$\frac{1}{C_A} = N1 - \frac{1}{C_B} > 0 \tag{6}$$

All possible solutions to Eq. 6 can be calculated to generate paired values for C_A and C_B to the desired degree of resolution. Equation 6 is written to solve for C_A in terms of

TABLE 2 Reliability analysis for the estimates of the impedance coefficients describing monolayer impedance

	Case 1*			Case 2#			Case 3§		
		Estimate			Estimate			Estimate	
	Actual	Mean	σ (%)	Actual	Mean	σ (%)	Actual	Mean	σ (%)
$N1$	0.954	0.953	0.20	0.742	0.742	0.19	0.987	0.987	0.35
$N0$	7.80×10^{-4}	7.85×10^{-4}	47.4	3.54×10^{-4}	3.55×10^{-4}	6.3	1.88×10^{-3}	1.88×10^{-3}	10.7
$D1$	3.41×10^{-3}	3.41×10^{-3}	11.6	2.59×10^{-3}	2.59×10^{-3}	1.3	4.63×10^{-3}	4.63×10^{-3}	4.8
R_m (Ω cm^2)	223			231			238		

The actual coefficients were derived from impedance measurements of HT29-Cl.16E monolayers under conditions as noted.
* Basal conditions.
# 1 min after purinergic stimulation.
§ 25 min after purinergic stimulation.

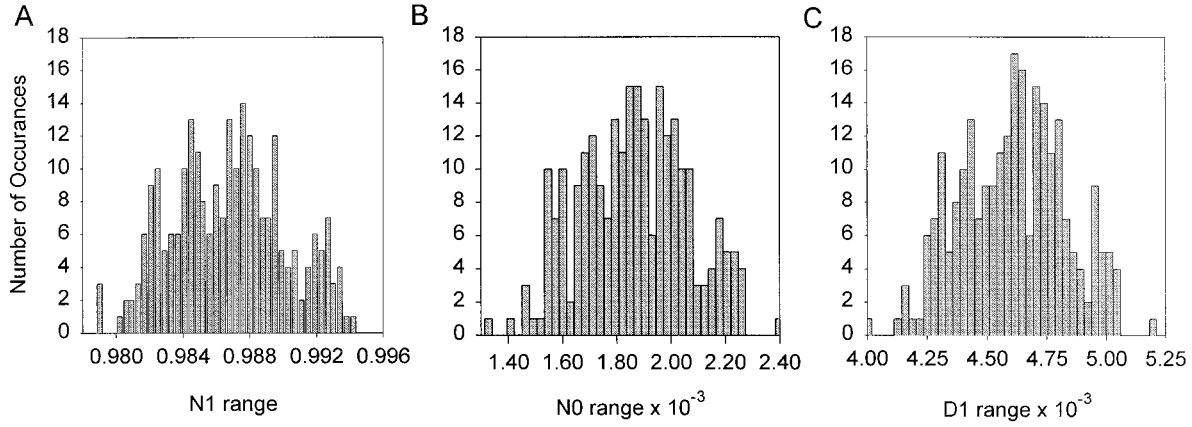

FIGURE 5 Confidence intervals and distribution of estimated impedance coefficients of Eq. 3 by Monte Carlo simulation. Noisy data were generated as described in Fig. 4 and impedance coefficients extracted from the noisy data by NWLS. The coefficients used to generate data represent case 3 of Table 2, i.e., 25 min after ATP stimulation; 250 simulations were performed. (*A*) range of $N1$ estimates, with actual $N1 = 0.987$; (*B*) range of $N0$ estimates, with actual $N0 = 1.88 \times 10^{-3}$; (*C*) range of $D1$ estimates, with actual $D1 = 4.63 \times 10^{-3}$.

C_B for this system as $C_B > C_A$. Only physically realizable values for the limits of C_B were used, with Table 1 serving as a guideline. There are now two equations (Eq. 4, b and c), in two unknowns (R_A and R_B), at each capacitance solution pair. These nonlinear equations can be solved for R_A and R_B at every capacitance solution pair. If the capacitance solution pair results in values of R_A or R_B that are not physically realizable (i.e., negative or more than three orders of magnitude change from the preceding measurement) then the capacitance pair is deemed out of its solution range.

This method was applied to a subset ($n = 10$) of the data shown in Fig. 5, using 5 μF/cm^2 $\leq C_B \leq$ 25 μF/cm^2 as limits (larger values of C_B did not produce solutions). As shown in Table 3, the span of estimates is defined by a minimal and maximal C_A, which represent the endpoints of a family of estimates in which the true value lies. Tests of the capacitance solution pair resolution (up to 500 increments) have shown that the endpoints represent the minimums and maximums of R_B as well, whereas R_A occasionally peaks midrange. Comparing the actual values used to generate the data in Fig. 5 with the range minimums and maximums in Table 3 gives $C_A \pm 1.5\%$, $R_A \pm 20\%$, $C_B \pm 10\%$, and $R_B \pm 8\%$.

Analog model circuit results

To test the performance of the estimation techniques using known components, an analog model circuit was tested. The full range of expected impedances (Table 1) was tested by inserting the appropriate resistors and capacitors in the circuit. Membrane parameter combinations mimicking the cases of Tables 2 and 3 produced results comparable in precision and accuracy to these Monte Carlo simulations. Reported here are the results of the worst-case parameter combination.

To simulate a worst-case parameter combination, model circuit parameter values were chosen so that the paracellular component dominates the impedance coefficient $D1$ (similar to case 1 of Table 2, i.e., HT29-Cl.16E monolayers under basal conditions). The estimation results of 10 separate tests are shown in Table 4. Comparing the actual impedance coefficients with the mean value of the estimates, accuracy is high for $N1$ (<1% difference) and $D1$ (1.5% difference) and lower for $N0$ (7.5%). This trend is the same as in the Monte Carlo simulations (see above). The standard deviations in the impedance coefficient estimates also followed the same trend as those of the Monte Carlo simulations, as shown in Tables 4 and 2, respectively. The model circuit results are within the estimated precision predicted by Monte Carlo analysis for cases where the paracellular component dominates $D1$.

The ranges of the membrane parameter values for these model circuit results were calculated from the estimated impedance coefficients. The average lower and upper endpoints of the range for C_A were -2% and $+20\%$, respectively, of actual; the solution space for R_A was smaller in this case than that predicted from Monte Carlo simulations (data not shown). The average value of R_m was 0.6% greater than calculated from the known components, with a standard deviation of 0.4%.

HT29-Cl.16E monolayer results

A series of tests were performed on HT29-Cl.16E monolayers to validate model selection and check for linearity and independence. The results of all parameter fits were subjected to tests of the residuals using the χ^2 goodness-of-fit test and a runs test. In all cases where the estimation was successful as deemed by convergence and the total minimized χ^2, tests of the residuals validated the fit at the 95% confidence interval. There were several cases during each experiment when the estimation was unsuccessful, failing to converge (8.3% of cases). For these cases, either the apparent noise profile deviated greatly from the estimated

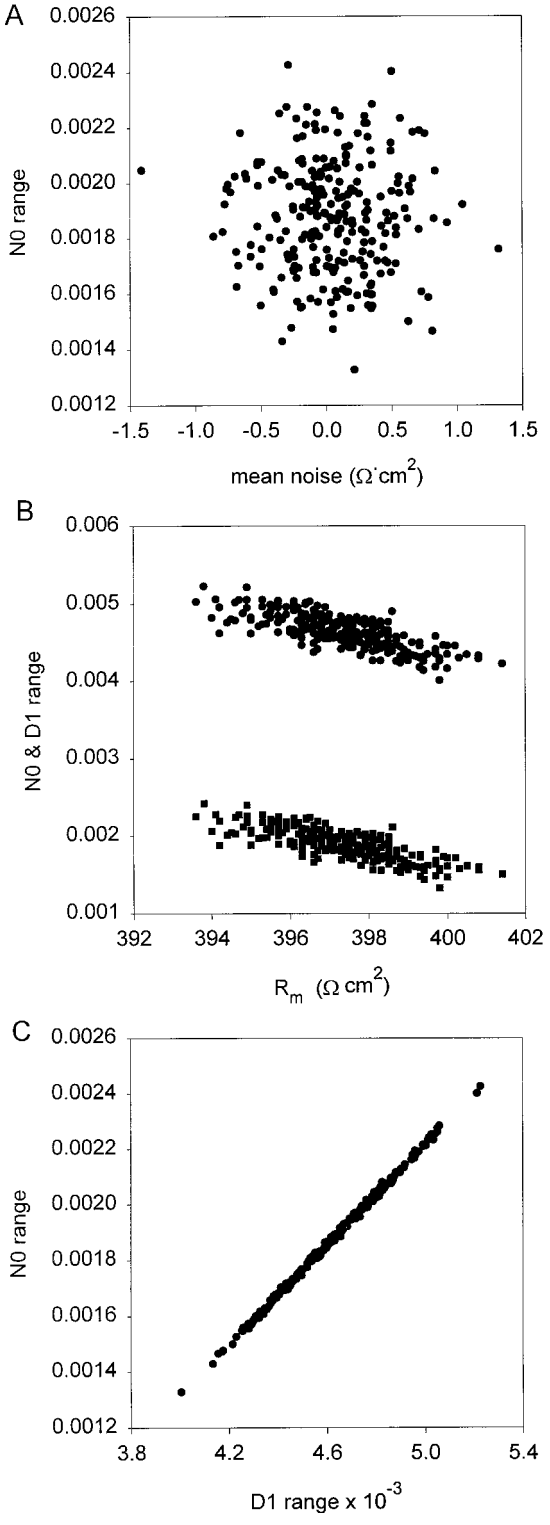

FIGURE 6 Correlation of estimated impedance coefficients with (*A*) mean noise, (*B*) R_m, and (*C*) each other. Note (*A*) absence of correlation between the value of *N*0 and the mean value of the noise added to the first 10 impedance samples (through 120 Hz), (*B*) modest correlation between the resistance-dependent impedance coefficients (*N*0 (●) and *D*1 (■)) and the total membrane resistance R_m, and (*C*) high correlation between the estimates of *N*0 and *D*1.

weights (>20%) or the baseline current (*Isc*) changed by >10% during the course of the measurement. To test for voltage independence, impedance measurements were performed at five different holding potentials representing the full range of expected variation. Each monolayer ($n = 4$) was subjected to all voltage levels consecutively, and the total capacitance was estimated for each case. A typical result is shown in Fig. 7. The data indicate that total capacitance is independent of the holding potential used.

Purinergically stimulated exocytosis experiments were performed on HT29-Cl.16E monolayers as a final test of the system to measure dynamic changes in capacitance and resistance of the individual membranes. A representative tracing of the inverse *N*1 coefficient (which represents the total monolayer capacitance) and R_m during the course of an experiment is shown in Fig. 8. The peak change in monolayer capacitance occurs within 1.5 min after ATP addition, with a gradual return to baseline during the next 20 min. The value of R_m rapidly increases during the 1st minute and then drops below its basal value, suggesting activation of membrane conductances. As these same values were used to perform the Monte Carlo simulations, the calculated tolerances and variations for those cases are expected to hold here.

The estimated coefficients were used to calculate membrane parameter ranges. An initial test using 5 μF/cm$^2 \leq C_B \leq 25$ μF/cm^2 as limits was performed; from these results, a minimal range of 5 μF/cm$^2 \leq C_B \leq 8.3$ μF/cm^2 was noted, and all ranges were recalculated using these limits as well. The resulting ranges are shown in Fig. 9, *A–C*. The change in apical capacitance (Fig. 9 *A*) mimics the changes in $N1^{-1}$ (Fig. 8), expected with $C_B > C_A$. Narrowing the range on C_B had minimal effect on the ranges of C_A and R_A, suggesting that the true value of C_B lies within this range throughout the experiment. Note that the narrowed range would still allow a 66% change in C_B. The resistance changes with time (Fig. 9, *B* and *C*) provide some interesting results. The minimal value of R_A is achieved at the capacitance maximum (1.25 min after ATP addition), and the decrease in R_A is briefly delayed with respect to the change in capacitance. Both observations are consistent with a portion of the apical membrane conductance being located in fusing granules (Merlin et al., 1996). The value of R_P appears to briefly increase after stimulation with ATP and then drops slightly after 2 min. The changes in R_P appear similar to the time course of R_m (Fig. 8). The solution ranges for both R_A and R_P increase 5 min after ATP stimulation; in this region, the high range of C_B begins to produce extreme and negative value changes in R_A, requiring truncation of the solution set. The ranges of R_B (not shown; can be calculated using Eq. 2) decrease in this same region.

DISCUSSION

Model selection

The ability to use the simplest model possible is a critical factor in dynamic impedance measurements. As model complexity increases, the requirements for auxiliary mea-

TABLE 3 Estimated ranges for membrane parameters

	Parameter range, low endpoint*				Parameter range, high endpoint*			
	C_A (μF/cm^2)	R_A (Ω cm^2)	C_B (μF/cm^2)	R_B (Ω cm^2)	C_A (μF/cm^2)	R_A (Ω cm^2)	C_B (μF/cm^2)	R_B (Ω cm^2)
Mean	1.98	1800	11.7	39.4	2.02	1247	10.4	44.2
σ	0.032	0[#]	1.00	6.3	0.031	54.3	0.82	7.0
SEM	0.011	0[#]	0.31	2.0	0.010	17.2	0.26	2.2
Actual	2.0	1500	10.8	42	2.0	1500	10.8	42
% difference	−1.1	+20	+8.2	−6.3	+1.2	−16.9	−4.2	+5.2

The mean value of $R_m = 238 \pm 1.0$ Ω cm^2; the corresponding impedance coefficients can be calculated using Eqs. 4, a–c.
* Low and high endpoints of C_A and R_B; the parameters C_B and R_A vary inversely to C_A and R_B, and R_A occasionally reaches a maximal mid-range. All values shown are minimums and maximums regardless of their location in the range.
[#] Solution range included the limit on $R_A = 1800$ Ω cm^2, from Table 1.

surements, longer measurement times, and assumptions that critical parameter values do not change increases. For example, the distributed model assumes that the apical membrane capacitance equals the exposed basolateral membrane capacitance, requires separate microelectrode measurements, and requires the use of sinusoidal stimulation signals (Clausen, et al., 1979). The capacitance assumption alone cannot be met when the experimental protocol is designed to effect large changes in the apical capacitance independent of the basolateral capacitance. The distributed model simplifies to the lumped model (Fig. 1 *A*) with the assumption that the lateral intercellular space (LIS) contribution to the paracellular pathway resistance is minimal, especially with respect to the junction resistance. This lumped model was chosen because 1) the HT29-Cl.16E subclone is a homogeneous population of cells with visible LIS and moderately tight junctions (200–500 Ω cm^2); 2) the LIS resistance has minimal effect on the apical parameters (Kottra and Frömter, 1984a,b), which are the primary components modified in these experiments; and 3) use of the distributed model has not resulted in an improved fit for other tissues in this impedance range (Clausen and Wills, 1981; Wills, 1984; Wills and Clausen, 1987).

In general, the lumped model does not take into consideration voltage dependencies of model parameters. However, total capacitance remains constant as the holding potential is varied over the full range expected during the experimental protocol, as shown in Fig. 7. Additional tests of the *I–V* response indicated that this epithelial cell line does not exhibit nonlinearities in current (and therefore resistance) as a function of voltage. Furthermore, in all cases that resulted in successful parameter estimation, tests of the residuals indicated that the model choice was sufficient to characterize the behavior of the data (Straume and Johnson, 1992a). Therefore, the lumped model appears well justified for the epithelial monolayer examined. These same tests (e.g., linearity, voltage independence, and normal residuals) must be applied to any epithelial monolayer using this system.

TABLE 4 Estimates of the impedance coefficients for model circuit measurements

		Estimate	
	Actual	Mean	σ (%)
$N1$	0.609	0.609	0.15
$N0$	2.00×10^{-4}	2.15×10^{-4}	11.3
$D1$	1.32×10^{-4}	1.34×10^{-4}	3.0
R_m (Ω cm^2)	387 (389)*	—	—

The actual impedance coefficients were derived from direct measurement of the components used in the model circuit, and calculated using Eq. 4, a–c. *The actual value of R_m from direct measurement of the components in the model circuit and Eq. 2 was 389 Ω cm^2; the mean value measured with the transepithelial voltage clamp was 387 Ω cm^2.

Transient analysis

Several different types of measurement signals have been used to perform impedance analysis. The earliest measurements were performed using square wave or transient analysis (Teorell, 1946); with the introduction of the distributed model, the technique of transient analysis was abandoned because the power spectral density over the frequency range needed to estimate the LIS morphological parameter specific to this model was inadequate (A/ℓ; Clausen et al., 1979). New methods were devised that relied on applying a discrete sum of frequencies simultaneously, either through summing sine waves of different frequencies or the use of circuits to generate pseudo-random noise (Clausen and Fer-

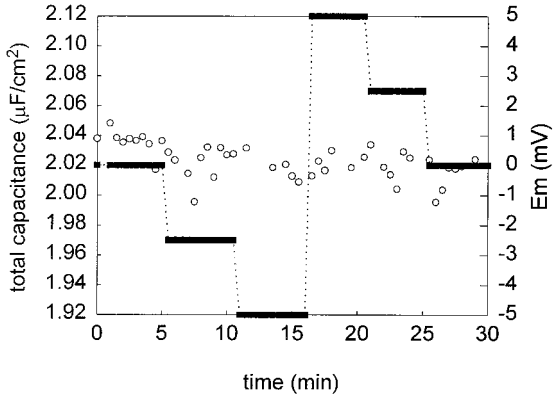

FIGURE 7 Independence of total monolayer capacitance on voltage. Total monolayer capacitance ($N1^{-1}$, ○) versus clamped holding potential (*Em*, ■). Capacitance axis limits represent ±5% of mean total capacitance.

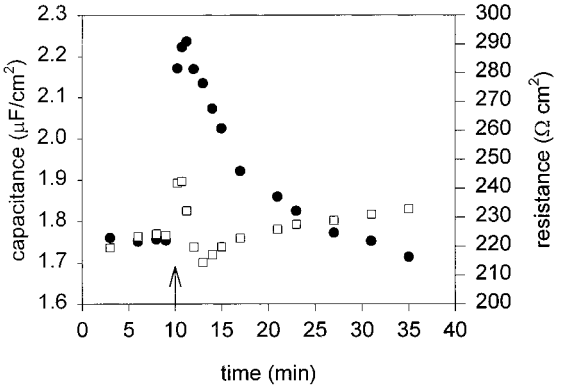

FIGURE 8 Representative tracings of estimated total monolayer capacitance ($N1^{-1}$, ●) and measured total membrane resistance (R_m, □) of HT29-Cl.16E monolayers stimulated with a purinergic agonist. A bolus of ATP was added apically at 10 min (*arrow*) to give a final concentration of 3 mM.

nandez, 1981; Kottra and Frömter, 1984a,b). These methods, however, require longer measurement times than the simple, transient pulse. As the lumped model does not use the LIS morphological parameter, transient analysis is adequate and provides the fastest measurement time.

Auxiliary measurements

The use of impedance analysis to estimate parameters in an epithelial monolayer has always relied on auxiliary measurements of at least one parameter to solve the mathematical relations. We have presented a system where substantial information can be ascertained without auxiliary measurements. The need for such a system is severalfold. The two most widely used techniques, microelectrode impalement (Kottra and Frömter, 1984a,b) and membrane permeabilization (Wills et al., 1979), are problematic in a dynamic measurement. For cells grown on permeable supports, microelectrodes must be placed through the apical membrane. The HT29-Cl.16E cells have numerous granules in the apical pole, making it difficult to place an electrode clearly in the cytoplasm. The potential for damage to the cell membrane structure is high, and during compound exocytosis membrane changes can affect electrode placement.

An amphotericin B permeabilization method has been used in other epithelia to estimate the paracellular resistance (Wills et al., 1979; Kottra and Frömter, 1990). Potentially, this method could provide auxiliary information that would allow interpretation of impedance data in terms of the additional four underlying cellular parameters (C_A, R_A, C_B, and R_B). Therefore, the use of the amphotericin B method was tested with HT29-Cl.16E monolayers but found to be problematic for several reasons. First, amphotericin B permeabilization appeared to affect more parameters than just the resistance of the membrane to which it was added. Second, the resistance changes with addition of amphotericin B were not linear with time, even for early time points, consistent with changes in electromotive forces for chloride

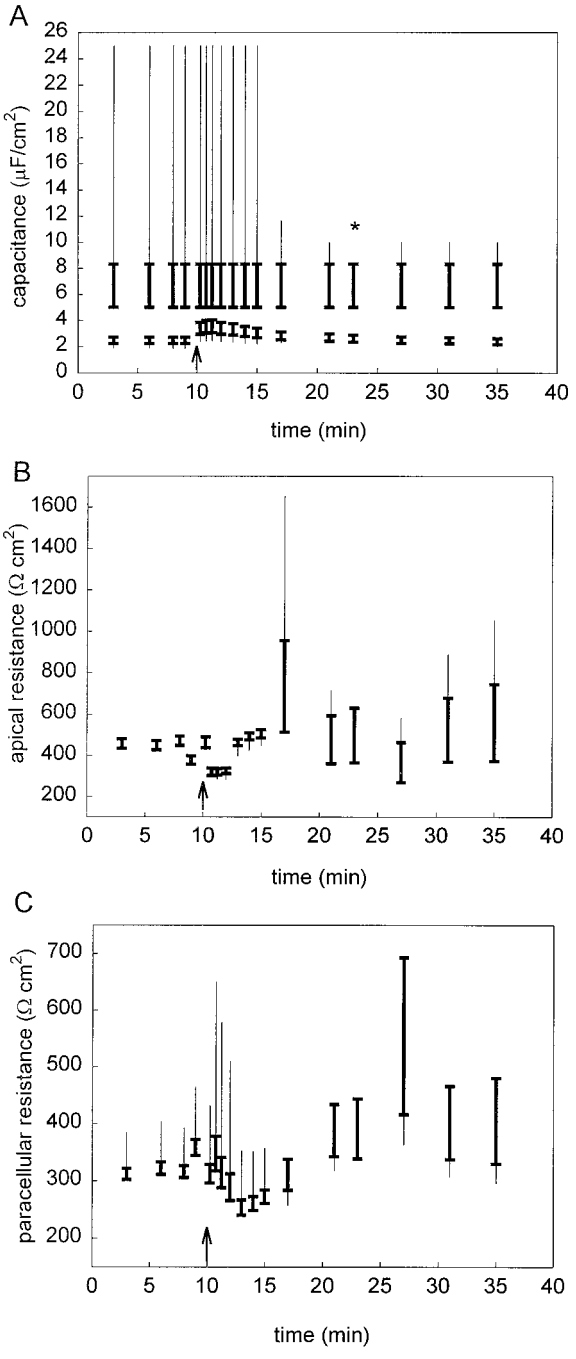

FIGURE 9 (*A*) Tracings of estimated apical (*lower trace*) and basolateral (*upper trace*) capacitance; (*B*) Estimated apical resistance; (*C*) Paracellular resistance ranges of HT29-Cl.16E monolayers stimulated with a purinergic agonist. ATP addition was as in Fig. 8. The thin lines are ranges calculated with typical C_B endpoints (5–25 μF/cm^2), whereas the thick lines are calculated with narrowed C_B endpoints (5–8.3 μF/cm^2). The narrowed range values were selected from results at 23 min (*asterisk in A*).

secretion across the apical membrane. In other words, the HT29-Cl.16E cells failed to fulfill two major criteria necessary for a valid interpretation of observations in terms of magnitude of the paracellular monolayer resistance (Kottra and Frömter, 1990).

Estimation results

The results of Fig. 8 clearly demonstrate that the course of exocytosis can be accurately monitored with this system. The brief increase in R_m that has been consistently observed during the first 1.5 min after ATP stimulation is most logically explained by an increase in R_P; the alternative would be for R_B to substantially increase while R_A remains high, an unlikely event given the magnitude of *Isc* increase seen after ATP. The results of Fig. 9 *C* also suggest an increase in R_P. Interestingly, this brief increase in resistance is not observed in whole-cell voltage clamp measurements of granule fusion after ATP stimulation in single 16E cells (Guo et al., 1997), also suggestive of involvement of R_P. In all cases, the precision in the *N*1 impedance coefficient gives an immediate measure of the degree and timing of exocytosis; as whole-cell voltage clamp techniques cannot distinguish between events in the apical or basolateral membranes, the value of *N*1 provides a comparable measure to these techniques for intact epithelial monolayers.

In the results of Fig. 9, ranges were recalculated using the narrowed limits for basolateral capacitance for several reasons. No difference in basolateral membrane is observed in electron micrographs of stimulated and basal 16E cell monolayers. No other factors that might greatly alter the basolateral membrane area have been identified. The range used still allows for a 66% variation in C_B, and the ranges of C_A and R_A were substantially unaffected by the narrowing of the range. The narrowed range substantially limits the range of R_P, which is expected to remain fairly consistent through an experiment.

Use of the model circuit confirms the ability of the voltage clamp to acquire impedance data in the short-circuit mode. The results indicate that acceptable estimates can be achieved even in this worst-case combination of realistic values for capacitors and resistors in the model circuit. In addition to simulating even the least sensitive parameter combination, the circuits exhibited similar standard deviations in the low-frequency components due to noise as in actual cell monolayers. The ability of this measurement and analysis system to estimate the membrane parameters given similar levels of noise in the region of greatest sensitivity of the impedance to parameter changes confirms the robustness of the estimation process. In addition, measurement of R_m was performed with consistently high tolerance.

As additional experiments are performed, it is anticipated that the viable ranges for parameters can be narrowed, in turn narrowing the solution range endpoints for all components. Perturbing the individual membrane conductances should confirm that the ranges observed in these tests are valid. Preliminary attempts to perturb the paracellular resistance suggest that R_A is in fact larger than R_P; such conclusions are also supported by other impedance measurement techniques in colon cells (Wills and Clausen, 1987; Wills, 1984). The high precision in measuring *N*1, the total monolayer capacitance, allows this system to directly compare magnitude and time course of exocytosis phenomena with those measured in single cells, providing a tool to probe these phenomena in intact monolayers.

APPENDIX A: MODEL EQUATIONS

In the lumped model (Fig. 1 *A*), five parameters describe the monolayer membrane characteristics, where R_A, C_A and R_B, C_B are the resistance and capacitance of the apical and basolateral membranes, respectively, and R_P is the resistance of the paracellular pathway. For an applied current $Im_T(t)$, the resultant membrane potential across the monolayer $Em_m(t)$ is the sum of the voltages across the capacitances ($V_A(t)$ across apical, $V_B(t)$ across basolateral). Using the voltages across the capacitances as the state variables, the state equations of the system are:

$$C_A \frac{dV_A(t)}{dt} = Im_T(t) - \frac{Em_m(t)}{R_P} - \frac{V_A(t)}{R_A} \quad (A.1)$$

$$C_B \frac{dV_B(t)}{dt} = Im_T(t) - \frac{Em_m(t)}{R_P} - \frac{V_B(t)}{R_B}, \quad (A.2)$$

where $V_A(t) + V_B(t) = Em_m(t)$. Applying the Laplace transform, these equations become:

$$C_A s V_A(s) = Im_T(s) - Em_m(s)/R_P - V_A(s)/R_A \quad (A.3)$$

$$C_B s V_B(s) = Im_T(s) - Em_m(s)/R_P - V_B(s)/R_B \quad (A.4)$$

These equations can be rewritten as:

$$Y_A(s) V_A(s) = Im_T(s) - Em_m(s)/R_P \quad (A.5)$$

$$Y_B(s) V_B(s) = Im_T(s) - Em_m(s)/R_P, \quad (A.6)$$

where $Y_A = (sC_A + 1/R_A)$, $Y_B = (sC_B + 1/R_B)$. Using the definition of $Em_m(t)$ with Eqs. A.5 and A.6, we can eliminate V_A and V_B to obtain:

$$Em_m(s) = Z_m(s) Im_T(s) \quad (A.7)$$

where

$$Z_m(s) = \frac{((Y_A + Y_B)R_P}{(Y_A Y_B R_P + Y_A + Y_B)} = \left(\frac{Y_A Y_B}{Y_A + Y_B} + \frac{1}{R_P}\right)^{-1} \quad (A.8)$$

Because electrodes cannot be exactly positioned at the monolayer surface, there is current flow through the adjacent fluid, constituting fluid resistance R_f, and a corresponding potential. The total membrane potential (Em_T) measured across the monolayer and fluid will include this potential:

$$Em_T(s) = (Z_m(s) + R_f) Im_T(s)$$

or

$$Em_T(s)/Im_T(s) = Z_m(s) + R_f = Z_T(s)$$

Under steady-state (DC) conditions ($t \to \infty$ or $s \to 0$):

$$Y_A(0) = 1/R_A,\ Y_B(0) = 1/R_B,$$

$$Z_m(0) = \left(\frac{1}{R_A + R_B} + \frac{1}{R_P}\right)^{-1} \equiv R_m,$$

and the transepithelial total resistance is given by:

$$Em_T(0)/Im_T(0) = Z_m(0) + R_f = Z_T(0) = R_m + R_f = R_T$$

When we substitute

$$\frac{1}{R_P} = \frac{1}{R_m} - \frac{1}{R_A + R_B}$$

and the definitions of $Y_A(s)$ and $Y_B(s)$ into Eq. A.8 we obtain Eq. 3 (see System Theory, above).

APPENDIX B: NOISE SIGNAL GENERATION

When equation-generated, noise-free data are used in the coefficient estimation procedure, absolute convergence is virtually guaranteed. The presence of noise in real data accounts for the variability in parameter estimation success. To accurately determine the confidence intervals for coefficient estimates using epithelial monolayer data, tests using equation-generated data must realistically reproduce expected noise variations. The following criteria were determined from the noise analysis and mathematically generated to produce a pattern similar to that in Fig. 3 *B*. First, the background noise in the monolayers is assumed to have a Gaussian distribution, with 0 mean and a standard deviation of 1–2 Ω cm^2. Second, the noise distributions in the real and imaginary components are independent (uncorrelated). Finally, a 60-Hz sine wave, with randomly varying phase (random variation of peak value in real and imaginary components), is present over the background noise.

The following technique was used to mathematically generate this pattern. A Gaussian-distributed, random number generator was used to create two separate, independent arrays of random numbers. One array was assigned as the real component (*RRN*), the other as the imaginary component (*IRN*). Next, a sine wave (*sw*) was generated in the time domain as

$$sw_i = A \sin\left(2\pi f \Delta t\, i + \frac{\pi}{\Delta P}\right),$$

where $A = 30\ \Omega$ cm^2, $f = 60$ Hz, $\Delta t = 40.7\ \mu$s, $i = 0 \ldots 2047$, and $\Delta P = 6(0.5 + RRN_1)$ with RRN_1 = the 1st value of *RRN*. These signals were added to the equation-generated data (Z_c) to generate noisy data (Z_c'):

$$Z_c' = \{Re(Z_c) + RRN + Re(\mathrm{FFT}(sw))\} + j\{Im(Z_c) + IRN + Im(\mathrm{FFT}(sw))\}$$

The random number generators created new arrays of values for each run of all Monte Carlo simulations.

We thank Dr. Stephen W. Jones for helpful discussions during the preparation of this manuscript.

This work was supported by National Institutes of Health grants DK 39658 (to U. Hopfer) and T32 HL07415 (to C. Bertrand), and in part by National Science Foundation Grant 9315886 (to D. Durand). We also acknowledge the Cystic Fibrosis Center Core grant DK-27651.

REFERENCES

Barnett, D. W., and S. Misler. 1997. An optimized approach to membrane capacitance estimation using dual-frequency excitation. *Biophys. J.* 72: 1641–1658.

Bertrand, C., D. Merlin, G. Saidel, and U. Hopfer. 1996. Measurement of granule fusion in an intact monolayer of HT29-Cl.16E. *FASEB.* 10: A494.

Chen, T. R. 1977. In situ detection of mycoplasma contamination in cell cultures by fluorescent Hoechst 33258 stain. *Exp. Cell Res.* 104: 255–262.

Clausen, C., and J. M. Fernandez. 1981. A low-cost method for rapid transfer function measurements with direct application to biological impedance analysis. *Pflügers Arch.* 390:290–295.

Clausen, C., S. A. Lewis, and J. M. Diamond. 1979. Impedance analysis of a tight epithelium using a distributed resistance model. *Biophys. J.* 26:291–318.

Clausen, C., and N. K. Wills. 1981. Impedance analysis in epithelia. *In* Ion Transport by Epithelia. Raven Press, New York.

Cole, K. S. 1968. Membranes, Ions, and Impulses. University of California Press, Berkeley, CA.

Debus, K., J. Hartmann, G. Kilic, and M. Lindau. 1995. Influence of conductance changes on patch clamp capacitance measurements using a lock-in amplifier and limitations of the phase tracking technique. *Biophys. J.* 69:2808–2822.

Gabel, R. A., and R. A. Roberts. 1980. Signals and Linear Systems. John Wiley and Sons, New York.

Gaisano, H. Y., M. Ghai, P. N. Malkus, L. Sheu, A. Bouquillon, M. K. Bennett, and W. S. Trimble. 1996. Distinct cellular locations of the syntaxin family of proteins in rat pancreatic acinar cells. *Mol. Biol. Cell.* 7:2019–2027.

Geddes, L. A., and L. E. Baker. 1967. The specific resistance of biological material: a compendium of data for the biomedical engineer and physiologist. *Med. Biol. Eng.* 5:271–293.

Guo, X., D. Merlin, R. D. Harvey, C. Laboisse, and U. Hopfer. 1995. Stimulation of Cl^- secretion by extracellular ATP does not depend on increased cytosolic Ca^{2+} in HT29-Cl.16E. *Am. J. Physiol.* 269: C1457–C1463.

Guo, X. W., D. Merlin, C. Laboise, and U. Hopfer. 1997. Purinergic agonists, but not cAMP, stimulate coupled granule fusion and Cl^- conductance in HT29-Cl.16E. *Am. J. Physiol.* 273:C804–C809.

Johnson, M. L. 1994. Use of least-squares techniques in biochemistry. *Methods Enzymol.* 240:1–22.

Kottra, G., and E. Frömter. 1984a. Rapid determination of intraepithelial resistance barriers by alternating current spectroscopy: experimental procedures. *Pflügers Arch.* 402:409–420.

Kottra, G., and E. Frömter. 1984b. Rapid determination of intraepithelial resistance barriers by alternating current spectroscopy: test of model circuits and quantification of results. *Pflügers Arch.* 402:421–432.

Kottra, G., and E. Frömter. 1990. Determination of paracellular shunt conductances in epithelia. *Methods Enzymol.* 191:4–27.

Laburthe, M., C. Augeron, C. Rouyer-Fessard, I. Roumagnac, J.-J. Maoret, E. Grasset, and C. Laboisse. 1989. Functional VIP receptors in the human mucus-secreting colonic epithelial cell line Cl.16E. *Am. J. Physiol.* 256:G443–G450.

Low, S.-H., S. J. Chapin, T. Weimbs, L. G. Kömüves, M. K. Bennett, and K. E. Mostov. 1996. Differential localization of syntaxin isoforms in polarized Madin-Darby canine kidney cells. *Mol. Biol. Cell.* 7:2007–2018.

Merlin, D., C. Augeron, X.-Y. Tien, X. Guo, C. L. Laboisse, and U. Hopfer. 1994. ATP-stimulated electrolyte and mucin secretion in the human intestinal goblet cell line HT29-Cl.16E. *J. Membr. Biol.* 137: 137–149.

Merlin, D., X. Guo, K. Martin, C. Laboisse, D. Landis, G. Dubyak, and U. Hopfer. 1996. Recruitment of purinergically stimulated Cl^- channels from granule membrane to plasma membrane. *Am. J. Physiol.* 271: C612–C619.

Peng, X.-R., X. Yao, D.-C. Chow, J. G. Forte, and M. K. Bennett. 1997. Association of syntaxin 3 and vesicle-associated membrane protein (VAMP) with H^+/K^+-ATPase-containing tubulovesicles in gastric parietal cells. *Mol. Biol. Cell.* 8:399–407.

Press, W. H., B. P. Flannery, S. A. Teukolsky, and W. T. Vetterling. 1986. Numerical Recipes: The Art of Scientific Computing. Cambridge University Press, Cambridge.

Riento, K., J. Jäntti, S. Jansson, S. Hielm, E. Lehtonen, C. Ehnholm, S. Keränen, and V. M. Olkkonen. 1996. A Sec1-related vesicle-transport protein that is expressed predominantly in epithelial cells. *Eur. J. Biochem.* 239:638–646.

Roumagnac, I., and C. Laboisse. 1987. A mucus-secreting human colonic epithelial cell line responsive to cholinergic stimulation. *Biol. Cell.* 61:65–68.

Schultz, S. G. 1980. Basic Principles of Membrane Transport. Cambridge University Press, Cambridge.

Straume, M., and M. L. Johnson. 1992a. Analysis of residuals: criteria for determining goodness-of-fit. *Methods Enzymol.* 210:87–105.

Straume, M., and M. L. Johnson. 1992b. Monte Carlo method for determining complete confidence probability distributions of estimated model parameters. *Methods Enzymol.* 210:117–129.

Teorell, T. 1946. Application of "square wave analysis" to bioelectric studies. *Acta Physiol. Scand.* 12:235–254.

Wills, N. K. 1984. Mechanisms of ion transport by the mammalian colon revealed by frequency domain analysis techniques. *In* Current Topics in Membranes and Transport. Academic Press, New York. 61–85.

Wills, N. K., and C. Clausen. 1987. Transport-dependent alterations of membrane properties of mammalian colon measured using impedance analysis. *J. Membr. Biol.* 95:21–35.

Wills, N. K., S. A. Lewis, and D. C. Eaton. 1979. Active and passive properties of rabbit descending colon: a microelectrode and nystatin study. *J. Membr. Biol.* 45:81–108.